Cytocidal macrophages in symbiosis with CD4 and CD8 T cells cause acute diabetes following checkpoint blockade of PD-1 in NOD mice

Hao Hu[a] [iD], Pavel N. Zakharov[a], Orion J. Peterson[a], and Emil R. Unanue[a,1]

[a]Division of Immunobiology, Department of Pathology and Immunology, Washington University School of Medicine in St. Louis, St. Louis, MO 63110

Autoimmune diabetes is one of the complications resulting from checkpoint blockade immunotherapy in cancer patients, yet the underlying mechanisms for such an adverse effect are not well understood. Leveraging the diabetes-susceptible nonobese diabetic (NOD) mouse model, we phenocopy the diabetes progression induced by programmed death 1 (PD-1)/PD-L1 blockade and identify a cascade of highly interdependent cellular interactions involving diabetogenic CD4 and CD8 T cells and macrophages. We demonstrate that exhausted CD8 T cells are the major cells that respond to PD-1 blockade producing high levels of IFN-γ. Most importantly, the activated T cells lead to the recruitment of monocyte-derived macrophages that become highly activated when responding to IFN-γ. These macrophages acquire cytocidal activity against β-cells via nitric oxide and induce autoimmune diabetes. Collectively, the data in this study reveal a critical role of macrophages in the PD-1 blockade-induced diabetogenesis, providing new insights for the understanding of checkpoint blockade immunotherapy in cancer and infectious diseases.

autoimmune diabetes | PD-1 blockade | exhausted CD8 T cells | monocyte-derived macrophages

Two of the most widely studied proteins that regulate T cell activation are cytotoxic T lymphocyte antigen 4 (CTLA-4) and programmed death 1 (PD-1). Inhibiting them can unleash regulatory controls of T cell activation, allowing the T cells to display their full functional potential. CTLA-4 and PD-1 are extensively studied in the cancer field, where their inhibitors—monoclonal antibodies—are used to treat cancer patients. Despite achieving success clinically, the checkpoint blockade immunotherapy can result in immune-related adverse events that frequently include endocrine autoimmune diseases (1), among them type 1 diabetes (T1D) (2–4). A recent comprehensive review summarized the clinical features of T1D induced by the immune checkpoint inhibition (4).

To better understand how PD-1 is regulating T1D, we examine here the nonobese diabetic (NOD) mouse model for changes in various cellular components following PD-1 blockade. PD-1 is synthesized de novo in activated T cells mediated by T cell receptor (TCR) signaling (5–7). Whereas PD-1 expression is rapidly up-regulated after antigen stimulation of naïve T cells, sustained TCR stimulation results in substantially higher expression of PD-1 and the establishment of T cell exhaustion in the examples of chronic viral infection and cancers (8–13). NOD mice with a gene knockout of PD-1 or treated with PD-1 blocking antibody develop accelerated autoimmune diabetes shown in a number of studies (14–21). Both autoreactive CD4 and CD8 T cells can respond to PD-1/PD-L1 blockade and contribute to the acute diabetes development (17–19). Central in this process is PD-L1 (the ligand of PD-1) expressed by the islet parenchymal cells (20, 21), which limits the T cell function in the islets and protects against autoimmune diabetes.

In this report we examine changes in various cellular components following PD-1 blockade by single-cell RNA sequencing

(scRNA-seq) and identify a previously unexplored islet macrophage population derived from monocytes with high proinflammatory activity. In the islets of anti–PD-1–treated mice, the infiltration by monocyte-derived macrophage (MoMac) was under the influence of CD4 and particularly CD8 T cells. The CD8 T cells largely comprised the precursor exhausted T (T_PEX) cells that were activated and differentiated to produce abundant IFN-γ in response to PD-1 blockade, which in turn activated the infiltrated MoMac to promote diabetes progression. The anti–PD-1 induced development of acute diabetes was reduced by restricting the infiltration and function of such MoMac in islets. Our study establishes that the myeloid cell compartment is an indispensable component of PD-1 regulation in autoimmune diabetes. Our study provides a cellular target, the MoMac, that may minimize the adverse effects of checkpoint blockade immunotherapy.

Results

Rapid Autoimmune Diabetes Develops after Immune Checkpoint Blockade of the PD-L1/PD-1 Pathway. We evaluated the effect of anti–PD-1 treatment in NOD mice during the early phase of the autoimmune process that starts at about third week of age, the time that initial T cells are present in islets, mostly in contact with the resident macrophages (ReMac) (22, 23). NOD mice of 6 to 8 wk of age treated with anti–PD-1 developed diabetes within 2 wk, whereas untreated mice became diabetic starting at around

Significance

Immune checkpoint inhibitors have achieved great success in the treatment of a number of malignancies. Unfortunately, immune-related adverse events develop in patients, particularly endocrine autoimmunity, including type 1 diabetes. We examined the nonobese diabetic mouse that develops fulminant autoimmune diabetes after anti–PD-1 blockade, uncovering an unexplored pathway by which PD-1 blockade facilitated diabetes progression. Analysis of the pancreatic islets showed strong cellular interactions among T cells and activated macrophages, and their dramatic changes after anti–PD-1 antibody treatment. Monocyte-derived macrophages played a major role in causing acute diabetes development. Their temporal depletion dramatically protected mice from β-cell demise. We identify the blood monocytes as a possible target for the control of the autoimmune complications brought about by checkpoint inhibitors.

20 wk of age (Fig. 1*A*), consistent with previous reports (16, 24). By histological examination, the islets of the mice treated with anti–PD-1 showed marked leukocytes infiltration compared to the nondiabetic untreated mice (Fig. 1*B*). Younger mice of 3 to 5 wk of age that have a limited number of infiltrating lymphocytes took longer to develop diabetes, in contrast to the 8- to 12-wk-old mice (*SI Appendix*, Fig. S1*A*).
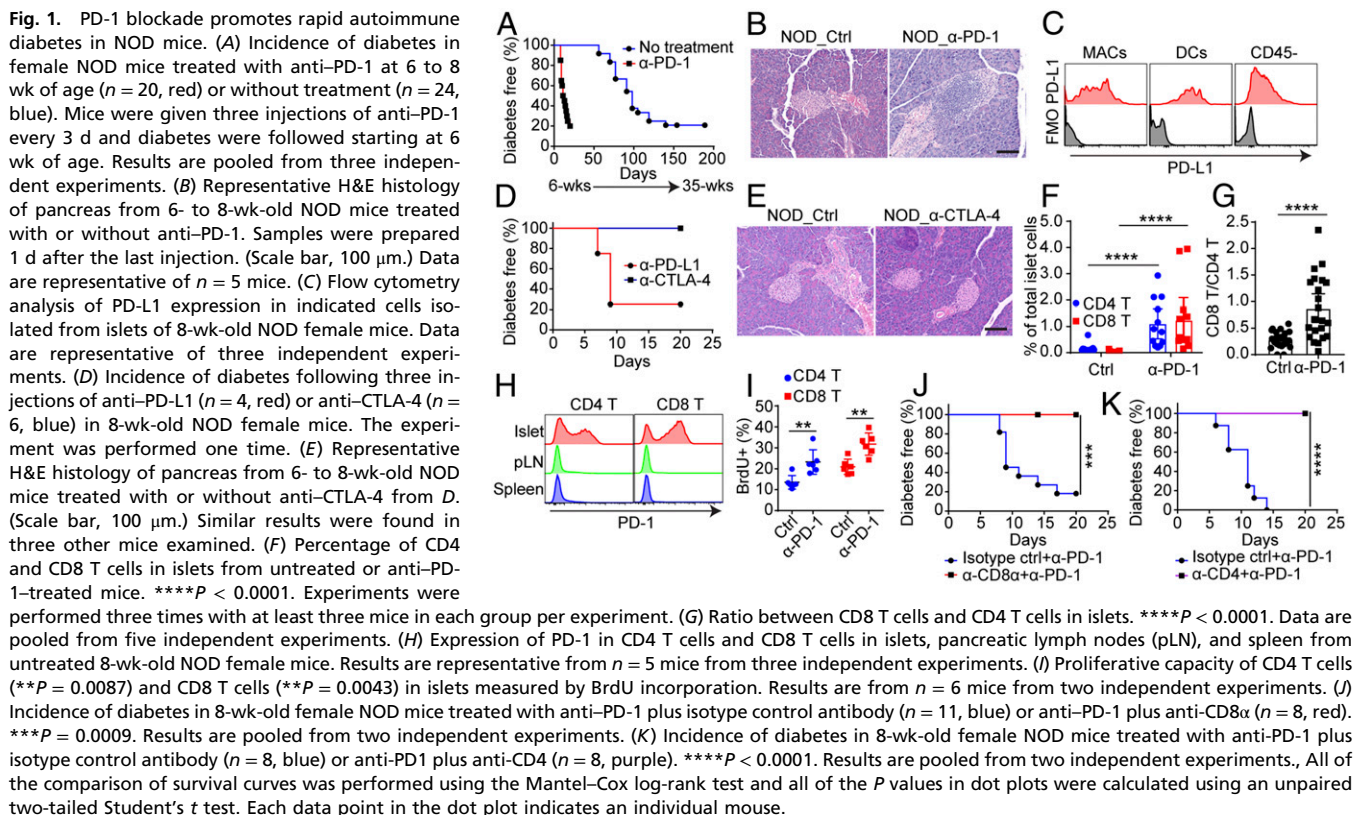
Autoimmune diabetes in NOD shows gender bias; in our colony only 25% of males develop diabetes, as opposed to ∼80% incidence among females. Anti–PD-1 treatment of 6- to 10-wk-old mice abolished this gender difference with both sexes equally developing diabetes (*SI Appendix*, Fig. S1*B*). Finally, of note is that around 20% of the NOD female mice in our colony do not develop diabetes when followed to 40 wk of age. The 40-wk-old nondiabetic NOD female mice that received anti–PD-1 acutely became diabetic even with only one injection of the antibody (*SI Appendix*, Fig. S1*C*). Thus, PD-1 regulation explains part of the gender bias, as well as the long-term resistance of many NOD mice to diabetes.

Islet ReMac, infiltrating dendritic cells (DC), and CD45⁻ cells, including the endocrine cells (mostly β-cells) and the endothelium, all expressed high levels of PD-L1 (Fig. 1*C*). Blockade of PD-L1 by anti–PD-L1 antibody also resulted in rapid diabetes development (Fig. 1*D*). However, CTLA-4 blockade failed to promote diabetes progression (Fig. 1 *D* and *E*), indicating that autoimmune diabetes was mainly controlled by the PD-1/PD-L1 axis. In sum, we confirmed that the PD-L1/PD-1 interactions had a profound controlling effect in autoimmune diabetes even from the early stages and extending to late stages.

Anti–PD-1 Treatment Enhances Islet Infiltration by CD4 and CD8 T Cells: Both Are Required for Diabetes Development. We evaluated the cellular response in islets from 6-wk-old NOD mice

following treatment with anti–PD-1 or isotype control antibody. Mice were killed 1 d after the last treatment; islets were isolated, and their cellular infiltrates were analyzed by flow cytometry. Both CD4 T cell and CD8 T cell numbers increased in anti–PD-1–treated mice compared with control mice (Fig. 1*F* and *SI Appendix*, Fig. S1*D*): The CD4 T cells increased about 4-fold but CD8 T cells had a more dramatic increase, about 40-fold, resulting in a sharp increase of CD8 T cell to CD4 T cell ratio (Fig. 1 *F* and *G* and *SI Appendix*, Fig. S1*D*). Of note, the level of CD8 T cells was always half of that of CD4 T cells in islets from mice with spontaneous diabetes, even at later stage. The majority of both CD4 T cells and CD8 T cells entering the islets expressed high levels of PD-1 at steady state in contrast to the T cells in the pancreatic lymph nodes and spleens (Fig. 1*H* and *SI Appendix*, Fig. S1*E*). Intraislet T cells displayed considerable cell division both in anti–PD-1–treated mice as well as in the controls assessed by BrdU incorporation (Fig. 1*I* and *SI Appendix*, Fig. S1*F*). However, in anti–PD-1–treated mice, both CD4 T cells and CD8 T cells incorporated more BrdU during the 7-d treatment than in control mice, showing higher proliferative response (Fig. 1*I* and *SI Appendix*, Fig. S1*F*).

CD4 T cells initiate the autoimmune responses in NOD diabetes followed by the involvement of CD8 T cells; both cells cooperate to promote the progression of diabetes (25, 26). Both CD4 and CD8 T cells also were under PD-1 regulation: Treatments that affected either CD4 T cells or CD8 T cells resulted in the loss of the diabetogenic effect of PD-1 blockade. For CD8 T cells, anti-CD8α (clone YTS169.4) reduced the CD8 T cell numbers in blood and pancreatic lymph nodes (*SI Appendix*, Fig. S1*G*) and completely abolished the diabetogenic effect of PD-1 blockade (Fig. 1*J*). For CD4 T cells, treatment with a nondepleting clone YTS177, which inactivates CD4 T cell function, resulted in a complete protection from anti–PD-1–induced diabetes (Fig. 1*K*).

Fig. 1. PD-1 blockade promotes rapid autoimmune diabetes in NOD mice. (*A*) Incidence of diabetes in female NOD mice treated with anti–PD-1 at 6 to 8 wk of age (*n* = 20, red) or without treatment (*n* = 24, blue). Mice were given three injections of anti–PD-1 every 3 d and diabetes were followed starting at 6 wk of age. Results are pooled from three independent experiments. (*B*) Representative H&E histology of pancreas from 6- to 8-wk-old NOD mice treated with or without anti–PD-1. Samples were prepared 1 d after the last injection. (Scale bar, 100 μm.) Data are representative of *n* = 5 mice. (*C*) Flow cytometry analysis of PD-L1 expression in indicated cells isolated from islets of 8-wk-old NOD female mice. Data are representative of three independent experiments. (*D*) Incidence of diabetes following three injections of anti–PD-L1 (*n* = 4, red) or anti-CTLA-4 (*n* = 6, blue) in 8-wk-old NOD female mice. The experiment was performed one time. (*E*) Representative H&E histology of pancreas from 6- to 8-wk-old NOD mice treated with or without anti-CTLA-4 from *D*. (Scale bar, 100 μm.) Similar results were found in three other mice examined. (*F*) Percentage of CD4 and CD8 T cells in islets from untreated or anti–PD-1–treated mice. ****P < 0.0001. Experiments were performed three times with at least three mice in each group per experiment. (*G*) Ratio between CD8 T cells and CD4 T cells in islets. ****P < 0.0001. Data are pooled from five independent experiments. (*H*) Expression of PD-1 in CD4 T cells and CD8 T cells in islets, pancreatic lymph nodes (pLN), and spleen from untreated 8-wk-old NOD female mice. Results are representative from *n* = 5 mice from three independent experiments. (*I*) Proliferative capacity of CD4 T cells (**P = 0.0087) and CD8 T cells (**P = 0.0043) in islets measured by BrdU incorporation. Results are from *n* = 6 mice from two independent experiments. (*J*) Incidence of diabetes in 8-wk-old female NOD mice treated with anti–PD-1 plus isotype control antibody (*n* = 11, blue) or anti–PD-1 plus anti-CD8α (*n* = 8, red). ***P = 0.0009. Results are pooled from two independent experiments. (*K*) Incidence of diabetes in 8-wk-old female NOD mice treated with anti-PD1 plus isotype control antibody (*n* = 8, blue) or anti-PD1 plus anti-CD4 (*n* = 8, purple). ****P < 0.0001. Results are pooled from two independent experiments., All of the comparison of survival curves was performed using the Mantel–Cox log-rank test and all of the P values in dot plots were calculated using an unpaired two-tailed Student's *t* test. Each data point in the dot plot indicates an individual mouse.

Depletion or inactivation of either CD8 T cells or CD4 T cells reduced the leukocyte infiltration of the islets (*SI Appendix*, Fig. S1*G*). The ratio of intraislet CD8 T cells versus CD4 T cells was also altered significantly (*SI Appendix*, Fig. S1*H*). B cell response was not affected in anti–PD-1–induced acute diabetes. Antiinsulin autoantibody titers did not change, nor was there an increase in T follicular helper cells in secondary lymphoid tissues (*SI Appendix*, Fig. S1 *I* and *J*). In sum, the numbers of both islet CD4 T cells and CD8 T cells were up-regulated by anti–PD-1, re-emphasizing the importance of both MHC class II and class I presentation in NOD diabetes development. Lacking either arm of the T cell immunity affected the autoimmune responses against β-cells.

scRNA-Seq Analysis Identifies Anti–PD-1 Responsive Islet Infiltrating Leukocyte. To further understand the cellular mechanisms of PD-1 immunoregulation in the islets, we performed scRNA-seq analysis of cells isolated from islets after anti–PD-1 treatment. Islet infiltrating leukocytes were isolated from 8-wk-old untreated NOD and anti–PD-1–treated NOD mice by flow cytometry sorting 1 d after the last injection of anti–PD-1 (Fig. 2*A*). The cells were subjected to 10X Genomics single-cell pipeline barcoding, library preparation, and sequencing. We performed a graph-based clustering to identify transcriptionally different leukocyte populations. In agreement with our recent study (27), clustering analysis revealed five major sets of leukocytes in the control and anti–PD-1–treated mice based on the expression of hallmark genes: T cells (both CD4 and CD8), B cells, conventional DCs (cDC), plasmacytoid DCs, and macrophages. In addition, we observed a set of proliferating leukocytes comprising several subsets (Fig. 2 *B* and *C*). B cells, CD4 T cells, and CD8 T cells were the predominant lymphoid cells but also included were a number of minor clusters of other lymphoid cells examined in our recent report (27). All clusters were identified in both control and anti–PD-1–treated conditions (Fig. 2*D*). DCs, macrophages, and T cells (especially CD8 T cells) were highly represented in the islets of anti–PD-1–treated mice, in contrast

to B cells (Fig. 2 *D* and *E*), confirmed in the flow cytometry analysis (Fig. 2*F*).

Examining CD4 T cells, we confirmed the presence of the five main clusters identified recently (27), based on their gene signatures (Fig. 3*A* and *SI Appendix*, Fig. S2 *A* and *B*, and Table S1). The five clusters included naïve T cells marked by *Lef1* and *Tcf7* expression; effector T cells marked by transcripts encoding cytokine *Ifng* and chemokine *Ccl5* expression; anergic T cells marked by the expression of inhibitory molecules *Cd200*, *Pdcd1*, *Lag3*; T regulatory cells (Treg) marked by *Foxp3* expression; and proliferating cells had up-regulated expression of cell cycle genes (Fig. 3*A* and *SI Appendix*, Fig. S2*B*). CD4 T cells showed no major population shifts in response to anti–PD-1 indicated by the relative abundance of each subset (Fig. 3 *B* and *C*). To note, anti–PD-1 did not affect the frequency of Tregs in the islets, also validated by flow cytometry (Fig. 2 *C* and *D*), suggesting a different control mechanism underlying PD-1 signaling.

We identified five major subpopulations of CD8 T cells by scRNA-seq (Fig. 3*E*), each characterized by unique gene signatures, including markers corresponding to various activation statuses (*SI Appendix*, Fig. S2 *C* and *D* and Table S2). As in the previous analysis, we found naïve cells (*Tcf7*, *Klf2*), XCL1$^+$ effector cells (*Xcl1*), proliferating cells (cell cycle genes), cytotoxic cells with high-level expression of genes encoding granzymes and killer cell receptors (*Gzma*, *Gznk*, *Klrk1*, *Klrc1*, and so forth), and exhausted T cells marked by the expression of *Pdcd1*, *Tox*, *Ctla4*, and *Lag3*. More CD8 T cells were found upon PD-1 blockade (Fig. 2*A*), but the relative proportion of all five clusters of CD8 T cells showed no major changes comparing control and anti–PD-1 samples (Fig. 3 *F* and *G*).

A Functional Alteration in Exhausted T Cells Occurs in Response to PD-1 Blockade. The exhausted CD8 T cells (T$_{EX}$) with a high level of PD-1 expression were shown to be the main target of PD-1 blockade in a chronic lymphocytic choriomeningitis viral (LCMV) infection model (28). Thus, we next examined by scRNA-seq for the possible heterogeneity of the exhausted CD8
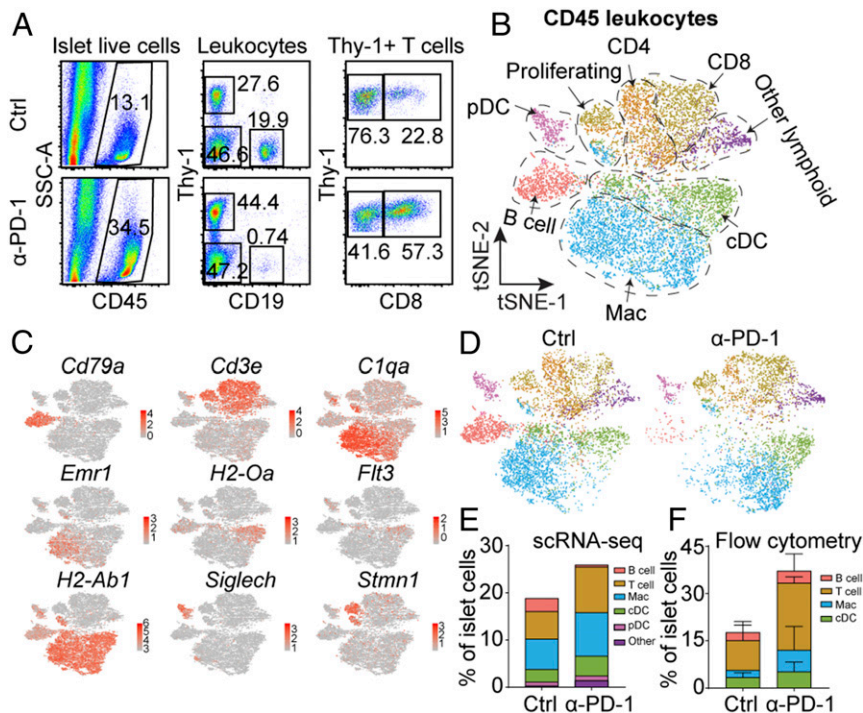
Fig. 2. scRNA-seq analysis identifies anti–PD-1 responsive islet infiltrating leukocytes. (*A*) Flow cytometry sorting of CD45$^+$ leukocytes from either 8-wk-old untreated mice or anti–PD-1–treated female mice. Mice were treated with three injections of anti–PD-1 antibody and islets were isolated 1 d after the third injection. (*B*) t-Distributed stochastic neighbor embedding (t-SNE) plot of intraislet leukocytes combining the 8-wk-old control and anti–PD-1–treated NOD mice. (*C*) Expression of canonical immune cell markers in clusters of islet-infiltrating leukocytes from *B*. (*D*) t-SNE plot from *B* split by the two conditions. (*E*) Fraction of immune cell populations relative to the total islet cells number in the two conditions calculated from scRNA-seq data. (*F*) Fraction of immune cell populations, including T cells, B cells, macrophages (Mac) and cDC relative to islet cells calculated based on flow cytometry analysis. The data came from individual mouse from four mice in each condition. Bars indicate SD.
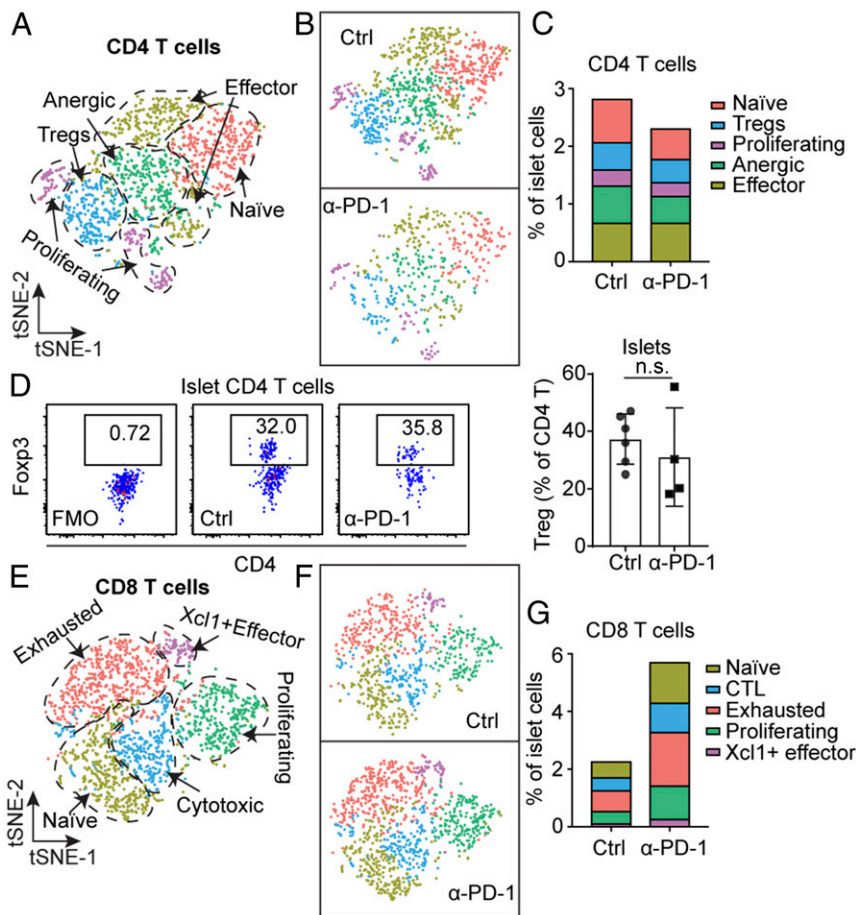
Fig. 3. Islet T cell heterogeneity after anti–PD-1 treatment. (*A* and *B*) *t*-SNE plot of intraislet CD4 T cells from the 8-wk-old untreated mice and anti–PD-1–treated mice described in Fig. 2; both are conditions merged (*A*) or shown separately (*B*). (*C*) Fraction of each cluster in CD4 T cells relative to total islet cells. (*D*) Flow cytometry analysis of Foxp3$^+$ Treg cells in islets treated with or without anti–PD-1, not significant (n.s., = 0.4762). Islets were examined on day 7 after the third injection of anti–PD-1. The result is representative of two independent experiments with $n = 2$ to 3 mice in each group. (*E–G*) Examination of CD8 T cells done as in *A–C*.

T cells in the islets from the control and anti–PD-1–treated mice. Previous studies had characterized two subsets of exhausted T cells based on TCF1 (encoded by *Tcf7* gene) expression, both having TOX as a common marker (29–31): TOX$^+$TCF1$^+$, the stem-like precursor (T$_{PEX}$) of the exhausted T cells and TOX$^+$TCF1$^-$, the terminally differentiated exhausted T cells (T$_{TEX}$) (32–34). In agreement with previous reports, we identified two subsets within the exhausted CD8 T cells (Fig. 4*A*). Importantly, the T$_{PEX}$ predominated in the control sample (over 75% of the exhausted T$_{EX}$ cells). In contrast, T$_{TEX}$ were highly represented in the anti–PD-1–treated condition, about 75% (Fig. 4*B*).

The T$_{TEX}$ subset was characterized by high levels of proinflammatory genes (*Nkg7*, *Ccl3*, *Ccl4*, *Ccl5*, *Gzmb*) (Fig. 4*C*). In T$_{PEX}$ we observed up-regulation of *Tcf7* and genes related to protein translation (*Rpl29*, *Rpl27a*, *Rpl35*, and *Eilf4g2*), and cell motility (*Tmsb10*) (Fig. 4*C*). By gene set enrichment analysis (GSEA) (35), the transcriptional signature of T$_{TEX}$ cells showed a strong statistical correlation (nominal $P < 1e\text{-}5$) with the transcriptional dataset on virus-specific CD8 T cells during chronic LCMV infection, the stem-like exhausted (PD-1$^+$ CD101$^-$Tim3$^-$) and terminally differentiated exhausted (PD-1$^+$ CD101$^+$Tim3$^+$) cells (36) (Fig. 4 *D* and *E*).

To further validate the two subsets of exhausted CD8 T cells detected by scRNA-seq analysis, flow cytometry analysis was performed on islets of 10-wk-old NOD mice. The two subsets of exhausted CD8 T cells were identified based on the expression of TOX and TCF1 in the islets: TOX$^+$TCF1$^+$: T$_{PEX}$ cells; and TOX$^+$TCF1$^-$: T$_{TEX}$ cells (Fig. 4*F* and *SI Appendix*, Fig. S3*A*). Compared to TOX$^-$ CD8 T (non-T$_{EX}$) cells, both exhausted

T cell subsets expressed high level of PD-1 and LAG3, consistent with scRNA-seq analysis (Fig. 4*F* and *SI Appendix*, Fig. S3*B*). We also examined other inhibitory molecules such as TIM3 and TIGIT, which were not detected by our scRNA-seq data but had been reported to express at a higher level in exhausted CD8 T cells. At protein level, both TIM3 and TIGIT showed an increased expression in exhausted CD8 T cells and T$_{TEX}$ revealed a higher level of TIM3 compared with T$_{PEX}$ (Fig. 4*F* and *SI Appendix*, Fig. S3*B*). Moreover, T$_{PEX}$ cells expressed high level of CXCR5, a maker of precursor exhausted T cells identified in a chronic LCMV infection model (33) (Fig. 4*F* and *SI Appendix*, Fig. S3*B*).

To further validate these results, we examined the expression of SLAMF6 and CD39, identified as surface markers of precursor exhausted T cells and terminally differentiated exhausted T cells, respectively (37, 38). PD-1$^+$ CD8 T cells were divided into SLAMF6$^+$CD39$^-$ and SLAMF6int/$^-$CD39$^+$ T cells (Fig. 4*G* and *SI Appendix*, Fig. S3*C*). SLAMF6$^+$ T cells expressed high level of TCF1, confirming they were T$_{PEX}$ cells. SLAMF6int/$^-$ T cells expressed a low level of TCF1 (Fig. 4*H*). Thus, SLAMF6 and CD39 could be used as the surrogate markers for TCF1 to differentiate T$_{PEX}$ and T$_{TEX}$ cells.

We examined the function of the CD8 T cells isolated from islets of 8- to 10-wk-old mice. The IFN-γ–expressing cells were determined after a 4-h culture with anti-CD3 and anti-CD28 antibody. While ~12% of the PD-1$^-$ nonexhausted T cells were IFN-γ$^+$, less than 5% of the exhausted T cells (T$_{PEX}$ or T$_{TEX}$) expressed IFN-γ, confirming they were bona fide exhausted T cells resistant to restimulation (Fig. 4*I* and *SI Appendix*, Fig. S3*D*).
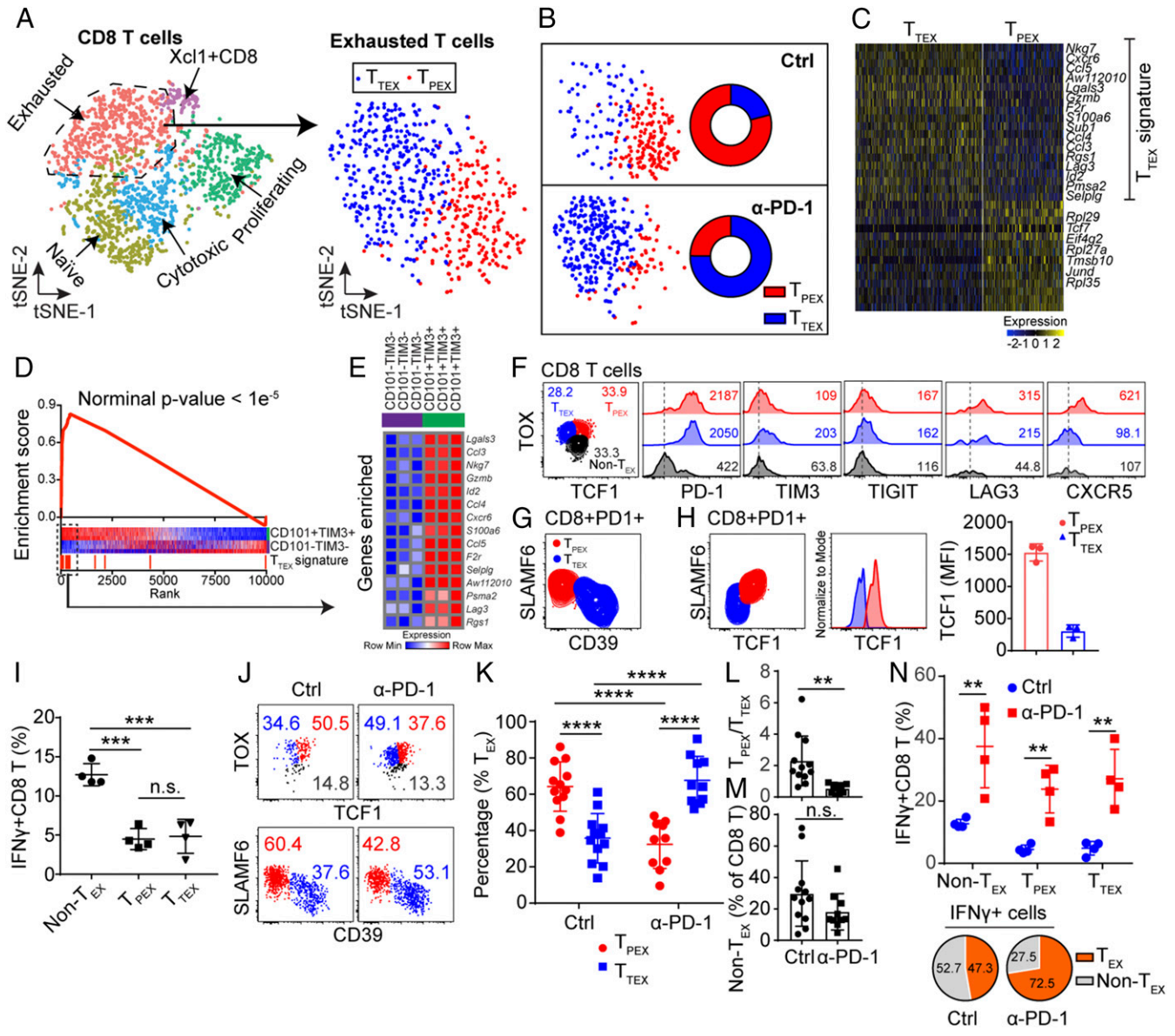
Hu et al.

Fig. 4. PD-1 blockade drives the functional alteration of exhausted CD8 T cells. (*A*, *Left*) t-SNE plot of CD8 T cells merged as in Fig. 3E. (*Right*) t-SNE plot of exhausted CD8 T cells extracted from the CD8 T cell population. (*B*) Population of exhausted cells from *A* split by the two conditions: T_{TEX} predominates after anti–PD-1 treatment. (*Right*) Quantification of the frequencies of each subpopulation. (*C*) Heat map illustrates the differences between two exhausted CD8 T cells subsets ($P_{adj} < 0.05$, Wilcoxon rank sum test). (*D*) GSEA plot comparing the T_{TEX} gene signature from *C* against published transcriptional dataset of exhausted CD8 T cells (BioProject: PRJNA497086) (nominal $P < 1e-5$). See text. (*E*) Heat map showing expression of enriched genes from *D* in the reference dataset used above. (*F*) Flow cytometry analysis of exhausted T cell in islets from 10-wk-old untreated NOD mice. Histogram shows the expression of key molecules associated with exhausted T cells, including PD-1 TIM3, TIGIT, LAG3, and CXCR5 (numbers in the box indicated mean fluorescent intensity). Flow analysis is representative from $n = 12$ mice from four independent experiments. The staining of each inhibitory molecule was repeated two to three times, as shown in *SI Appendix,* Fig. S3B. (*G*) Flow cytometry analysis of T_{PEX} and T_{TEX} cells examining for SLAMF6 and CD39. Results are representative from $n = 3$ mice. (*H*) Expression of TCF1 in SLAMF6$^+$ T_{PEX} and SLAMF6$^-$ T_{TEX} and quantification of TCF1 expression in each subset. Data are representative from $n = 3$ mice. (*I*) IFN-γ expression in T_{PEX}, T_{TEX}, and non-T_{EX}. (T_{PEX} vs. non-T_{EX}) ***$P = 0.0002$, (T_{TEX} vs. non-T_{EX}) ***$P = 0.0009$, n.s., $= 0.7947$. Results are pooled from $n = 4$ mice from two independent experiments. (*J*) Flow cytometry analysis using TOX and TCF1 (*Upper*) and SLAMF6 and CD39 (*Lower*) to examine the distribution of T_{PEX} cells and T_{TEX} cells in control and anti–PD-1–treated 8-wk-old NOD mice. Data are representative from two independent experiments in each staining protocol. (*K*) Percentage of T_{PEX} cells and T_{TEX} cells by each condition, pooled from the results of the two staining protocols in *J*. ****$P < 0.0001$. Each dot represents one experiment. (*L*) Ratio of T_{PEX} cells and T_{TEX} cells based on the results of *K*. **$P = 0.0024$. (*M*) Percentage of non-T_{EX} cells in control and anti–PD-1–treated mice, taken from the results in *J*, n.s., $= 0.1331$. (*N*, *Upper*) IFN-γ expression in T_{PEX}, T_{TEX}, and non-T_{EX} under the indicated treatment. **$P = 0.0097$ (non-T_{EX}), **$P = 0.0025$ (T_{PEX}), **$P = 0.0037$ (T_{TEX}). (*Lower*) Pie chart indicating the percentage of IFN-γ^+ cells from nonexhausted T cells and exhausted T cells in each condition. Results are pooled from $n = 4$ mice from two independent experiments.

Since scRNA-seq data revealed that T_{PEX} cells consisted of most of the exhausted T cells in the control sample and T_{TEX} was the major subset in the anti–PD-1–treated sample (Fig. 4B), it indicated that anti–PD-1 treatment promoted the differentiation of precursor cells to terminally differentiated cells, as shown in previous studies (36, 37, 39–41). To validate this result, 7-wk-old NOD mice were treated with three injections of anti–PD-1 for 1 wk or left untreated, islets were isolated at day 7 (mice were

8-wk-old) after the first injection and CD8 T cells were examined by flow cytometry. The two different staining protocols (TOX/TCF1 and SLAM6/CD39) were used to identify T_{PEX} and T_{TEX} in control mice or anti–PD-1–treated mice. In agreement with scRNA-seq data, TOX^+TCF1^+ T_{PEX} cells predominated in control islets whereas TOX^+TCF1^- T_{TEX} cells were highly represented in anti–PD-1–treated islets (Fig. 4 *J, Upper*). The same phenomenon was observed when SLAMF6 and CD39 were used to mark the two subsets of the exhausted T cells (Fig. 4 *J, Lower*).

Combining the results obtained from the two different staining protocols, 60% of the exhausted CD8 T cells were T_{PEX}, whereas 40% of them were T_{TEX} cells in control islets (Fig. 4*K*), reflecting the same subset distribution acquired from scRNA-seq data. On the other hand, the T_{TEX} cells were significantly expanded in all mice treated with anti–PD-1, accounting for 70% of the T_{EX} cells (Fig. 4*K*). The phenotypic divergence on T_{EX} cells induced by PD-1 blockade was better documented by examining the ratio between T_{PEX} and T_{TEX} cells with or without anti–PD-1 treatment (Fig. 4*L*). As in untreated control mice, the ratio scattered between 1 and 6; upon anti–PD-1 treatment, the ratio was mostly lower than 1 and very tightly distributed (Fig. 4*L*), suggesting a potent alteration induced by anti–PD-1 treatment. More importantly, the non-T_{EX} was a minor component of the islet CD8 T cells in both conditions and the proportion of non-T_{EX} following PD-1 blockade showed a trend of reduction, although it did not reach a significance (Fig. 4*M*).

To further examine these changes in the CD8 T cells response to anti–PD-1, we then tested for IFN-γ expression as is shown in Fig. 4*I*, but now including the anti–PD-1–treated mice. Islets from anti–PD-1 or control-treated mice were isolated and IFN-γ expression was examined ex vivo among the CD8 T cells after a 4-h culture with anti-CD3 and anti-CD28 antibody. There was a definite increase of IFN-γ expression in all subsets of the CD8 T cells, including non-T_{EX} T cells, T_{PEX} cells, and T_{TEX} cells (Fig. 4 *N, Upper* and *SI Appendix*, Fig. S3 *D and E*). In brief the anti–PD-1 treatment had rescued the limited response of the exhausted T cells. Given that exhausted CD8 T cells represented the major subset after PD-1 blockade, we estimated that about 70% of the IFN-γ–producing cells were derived from exhausted CD8 T cells in anti–PD-1–treated mice (Fig. 4 *N, Lower*). Thus, anti–PD-1 cultivated an IFN-γ ample microenvironment.

A Distinct Subset of Islet Macrophages Expands in Response to Anti–PD-1. In response to PD-1 blockade, myeloid cells underwent a striking remodeling, shown by scRNA-seq analysis (Fig. 5*A*). For DCs, we identified conventional DC1 with a high level of *Xcr1* expression, and three subsets of conventional DC2 (*SI Appendix*, Fig. S4 *A–C*), in agreement with our recent study (27). Both cDC1 and cDC2 were present in control and anti–PD-1 conditions (*SI Appendix*, Fig. S4*D*). While cDC contained a superimposed inflammatory signal after PD-1 blockade, manifested by IFN-γ inducible genes such as *Cxcl9* (Fig. 5 *A and B* and *SI Appendix*, Fig. S4*A*), the cellular composition in the cDC cohort underwent only mild changes (*SI Appendix*, Fig. S4 *C–E*).

scRNA-seq analysis of islet macrophages confirmed the presence of the four major clusters identified in our recent scRNA-seq examination of islets through diabetes progression (27) (Fig. 5*A* and *SI Appendix*, Fig. S4*A*). Macrophages from control islets were mostly populated by cluster Mac-1 (Apoe) and Mac-2 (Atf3) (Fig. 5 *B and C*). Briefly, the Mac-1 (Apoe) cluster was characterized by its expression of classic macrophage maturation genes, such as *Apoe*, *C1qa*, *Emr1* (encodes F4/80), and absence of a proinflammatory signature. The Mac-2 (Atf3) cluster was characterized by the expression of genes with NF-κB activation signatures, such as *Jun*, *Fos*, *Atf3*, and so forth. (Fig. 5*D*). Both clusters were also found in NOD.*Rag1*$^{-/-}$ mice (27), indicating

their homeostatic role under physiological conditions. Mac-3 cluster was characterized by the high expression of IFN-γ signature genes—including *Stat1*, *Cxcl9*, *Cxcl10*, *Isg15*—and also displayed signatures of NF-κB activation (Fig. 5*D*). This subset increased during the progression of diabetes but was absent in NOD.*Rag1*$^{-/-}$ mice (27), indicating their association with an active autoimmune response. A minor cluster, Mac-4, was characterized by higher expression of *Prdx-1*, and potential antiinflammatory activity (Fig. 5 *A and D*); it was down-regulated during the development of the diabetes in NOD mice (27).

Macrophages underwent marked changes in their subset distribution after anti–PD-1 treatment. Our attention was drawn to the Mac-3 (Cxcl9) cluster of highly activated macrophages that outnumbered the other subsets following PD-1 blockade (Fig. 5 *B and C*). The Mac-3 (Cxcl9) macrophages were further separated into two subsets with distinct gene signatures: A resident subset, Mac-3-R, and a monocyte derived subset, Mac-3-M (Fig. 5 *A and D*). Compared with Mac-3-R, Mac-3-M expressed higher levels of *Ly6c1*, *Ly6c2*, *Ccr2*, and *Il1rn*, and lower levels of *Emr1* and *Cx3xr1* (Fig. 5*E*), consistent with a monocyte derivation. In addition, many of the genes involved in IFN-γ and NF-κB gene signatures exemplified by *Cxcl9*, *Cxcl10*, *Stat1*, *Il1b* and so forth, were further up-regulated in Mac-3-M, showing a higher proinflammatory activity (Fig. 5*E*). Mac-3-M represented half of the islet macrophages following PD-1 blockade compared to its low frequencies in control islets (Fig. 5 *B and C*).

Flow cytometry analysis of islets after anti–PD-1 treatment validated the two subsets of Mac-3 (Cxcl9) identified by scRNA-seq. We observed an increased infiltration of $Ly6C^+F4/80^{lo}$ MoMac following PD-1 blockade compared with control mice in which $Ly6C^-F4/80^+$ ReMac predominated (Fig. 5*F* and *SI Appendix*, Fig. S4*F*). Consistent with the scRNA-seq data, MoMac expressed higher level of *Ccr2* and MHC-II molecule *I-A*^{g7} and lower levels of *Emr1* and *Cx3cr1* at the protein level relative to ReMac (Fig. 5*G*). In brief, the MoMac was compatible with the Mac-3-M subset and the ReMac comprised the Mac-3-R identified in the scRNA-seq.

T cells were responsible for the recruitment of MoMac cells. When CD4 T cells or CD8 T cells were inactivated or depleted by antibody treatment, PD-1 blockade failed to recruit MoMac into the islets (Fig. 4 *F and H*), and as is shown in Fig. 1, diabetes development was compromised (Fig. 1 *J and K*). Important to note, the infiltration by MoMac cells was also found in the late-prediabetic stage during natural diabetes development. MoMac cells were abundantly recruited in islets from 16-wk-old NOD mice, just before diabetes was manifested, while their representation was low at 6-wk of age (*SI Appendix*, Fig. S4*G*). There were no changes in the distribution of the spleen monocytes or red pulp macrophages at the two ages (*SI Appendix*, Fig. S4*H*).

These data support the concept that T cells were responsible for the recruitment and activation of the MoMac following anti–PD-1 treatment. The MoMac as well as the ReMac received numerous signals mainly derived from IFN-γ and committed to proinflammatory programs.

MoMac Are More Proinflammatory Compared with Islet ReMac. scRNA-seq analysis revealed that Mac-3-M showed a more profound proinflammatory activity (higher level of IFN-γ signature) compared with Mac-3-R (Fig. 5*E*). To validate this observation, islets were isolated from older 10- to 12-wk-old NOD mice, a time in which they were already heavily infiltrated with T cells and contained a level of MoMac cells (*SI Appendix*, Fig. S5 *A and B*). The islets were cultured with control antibody or with anti–PD-1 antibody for 48 h and examined. Following PD-1 blockade, we detected a higher level of IFN-γ secreted from the islets (Fig. 6*A*), making the point that anti–PD-1 directly
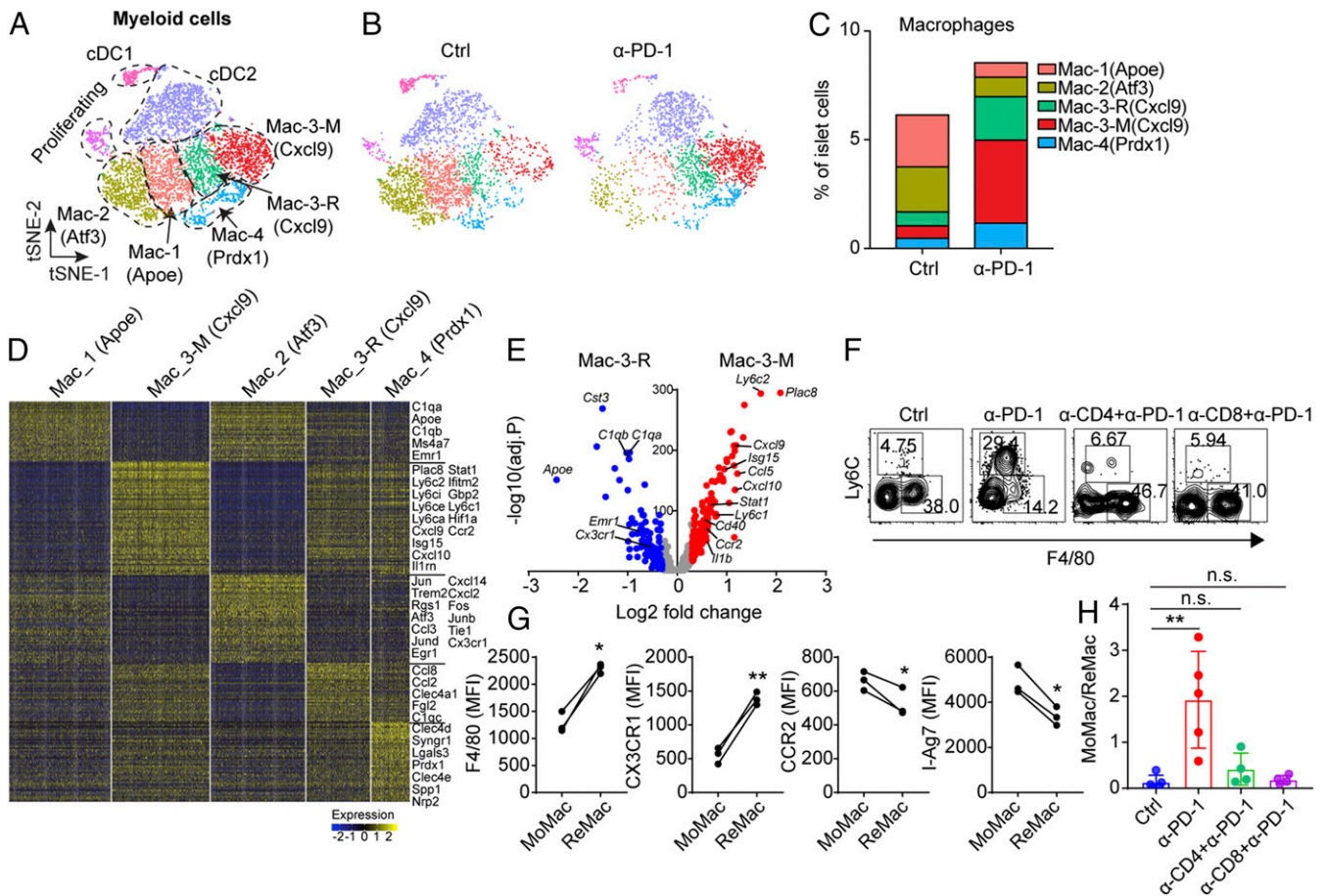
Fig. 5. PD-1 blockade drives the infiltration of MoMac into islets. (*A*) Combined *t*-SNE plot of myeloid cells obtained from 8-wk-old untreated and anti–PD-1–treated NOD female mice. Dashed lines encompass the general populations containing DC-1, DC-2, proliferating cells, and four clusters of macrophages. (*B*) *t*-SNE plot from *A* split by the two conditions. (*C*) Fraction of each cluster of macrophages relative to all islet cells in the two conditions. (*D*) Heat map showing the differential expression gene analysis among subsets of macrophages ($P_{adj} < 0.05$, Wilcoxon rank sum test). (*E*) Volcano plot shows the differential gene expression between Mac-3-R and Mac-3-M ($P_{adj} < 0.05$, Wilcoxon rank sum test). (*F*) Flow cytometry validating the infiltration of MoMac under the indicated treatment. Data are representative of four independent experiments. (*G*) Expression of several protein marker comparing MoMac and ReMac in islets from 8-wk-old NOD female mice (*n* = 3). (F4/80) *P = 0.0123, (CX3CR1) **P = 0.0053, (CCR2) *P = 0.0445, (I-A^{g7}) *P = 0.0119. P value is calculated using a paired two-tailed Student's *t* test. (*H*) Ratio between MoMac and ReMac in islets compared among different conditions. Control refers to untreated mice. **P = 0.0079, n.s. (Ctrl vs α-CD4+α-PD-1), = 0.1380, n.s. (Ctrl vs α-CD8+α-PD-1), = 0.5390. Results are pooled from two independent experiments.

activated the intraislet T cells to produce more IFN-γ. Macrophages activated by IFN-γ can release bioactive molecules that can affect surrounding cells. The most prominent one is nitric oxide (NO), resulting from the expression of the induced nitric oxide synthase (iNOS), encoded by the *Nos2* gene. The expression of iNOS is controlled by NF-κB at steady state and can be augmented by IFN-γ signaling (42). Following anti–PD-1, more of the islet macrophages but not the DC expressed iNOS (Fig. 6*B* and *SI Appendix*, Fig. S5 *C* and *D*).

We compared the expression of iNOS between the ReMac lacking Ly6C expression and the infiltrated MoMac with high Ly6C expression in the isolated islets. Both sets responded to anti–PD-1 antibody to express a higher level of iNOS (Fig. 6 *C* and *D* and *SI Appendix*, Fig. S5*E*). However, more of the MoMac expressed iNOS either with or without anti–PD-1 (Fig. 6 *E* and *F*), suggesting that the MoMac cells were inherently more active than ReMac in islets. The activation of macrophages was dependent on IFN-γ signaling as islet macrophages from IFNγR1$^{-/-}$ mice had no iNOS expression in response to anti–PD-1 (Fig. 6*G* and *SI Appendix*, Fig. S5*C*). In sum, islet macrophages, especially infiltrated MoMac, became highly activated in response to IFN-γ produced by T cells after PD-1 blockade.

Depletion of MoMac Inhibits the Development of Diabetes Induced by PD-1 Blockade. Treatment of mice with clodronate liposomes depleted monocytes in blood (*SI Appendix*, Fig. S6 *A* and *B*) but not the islet ReMac (*SI Appendix*, Fig. S6 *C–E*). Clodronate liposome-treated mice showed reduced monocyte infiltration into islets following PD-1 blockade, albeit not to the baseline level (Fig. 7 *A* and *B*). The mice also showed a reduction in total leukocytes infiltration (Fig. 7*C*). Activated monocytes expressed a high level of *Cxcl9* and *Cxcl10* (Fig. 5*E*), chemoattractants that recruit T cells, and their reduction might be the cause for the drop in leukocyte infiltration. The clodronate liposome-treated mice were protected from anti–PD-1–induced autoimmune diabetes (only 20% became diabetic), in contrast to almost all of the control mice (Fig. 7*D*). Thus, blocking the infiltration of the monocyte into islets restricted the diabetogenicity induced by PD-1 blockade.

In an effort to understand the pathways by which macrophages were involved in the induction of diabetes after anti–PD-1 antibody treatment, we considered the role of interferons as well as the means by which the recently arrived macrophages affected diabetogenesis. Since both subsets of Mac-3 macrophages had transcriptional signatures associated with strong IFN-γ signaling,
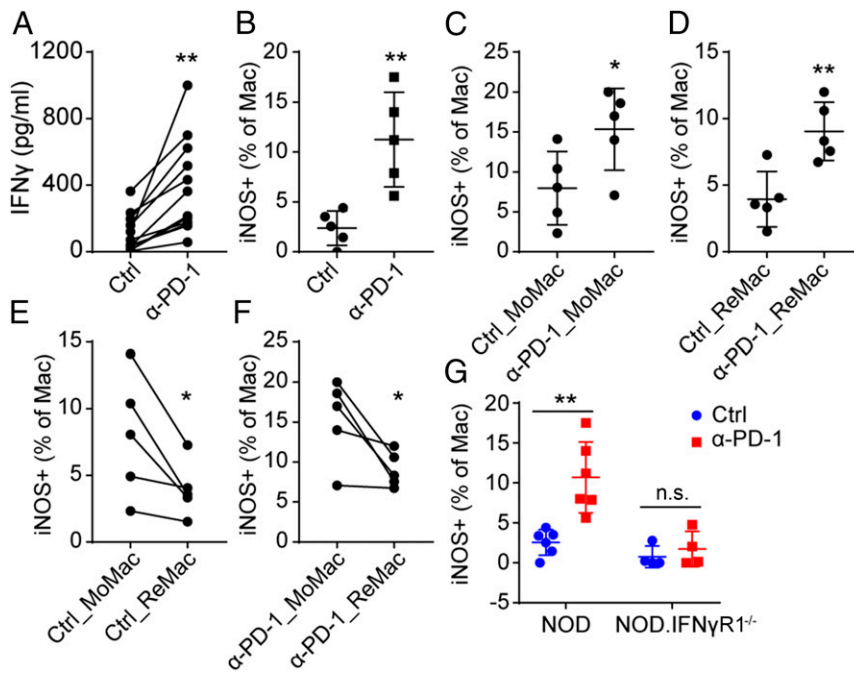
Fig. 6. MoMac are more proinflammatory compared with islet ReMac. (*A*) Quantification of IFN-γ production in supernatants from 100 cultured islets isolated from 10- to 12-wk-old NOD mice from 12 independent experiments (each data point). Islets were cultured for 48 h with or without anti–PD-1 antibody (50 μg/mL). **P = 0.0018, P value was calculated using a paired two-tailed Student's t test. (*B*) Expression of iNOS in macrophages from islets cultured with or without anti–PD-1 for 48 h as in *A*, from five independent experiments. Islets were dispersed and the expression of iNOS was examined by flow cytometry. **P = 0.0022. (*C*–*F*) Expression of iNOS in MoMac or resident macrophages with or without anti–PD-1 treatment. (*C*) *P = 0.0438, (*D*) **P = 0.0055, (*E*) *P = 0.0411, (*F*) *P = 0.0427. P values of *E* and *F* were calculated using a paired two-tailed Student's t test. (*G*) Expression of iNOS in macrophages from 100 islets isolated from 10- to 12-wk-old NOD wild-type mice or NOD.IFNγR1$^{-/-}$ mice. **P = 0.0017, n.s., = 0.4768. Results are pooled from two independent experiments with two to three mice from each group per experiment.

we treated NOD mice deficient in *Ifnar1* (NOD.IFNαR1$^{-/-}$) or *Ifngr1* (NOD.IFNγR1$^{-/-}$) or both *Ifnar1* and *Ifngr1* (NOD.DKO) encompassing a wide range of ages, from 5 wk to 16 wk, with anti–PD-1 blocking antibody. Both NOD wild-type mice and NOD.IFNαR1$^{-/-}$ mice developed diabetes rapidly. However, mice lacking IFN-γ signaling (NOD.IFNγR1$^{-/-}$ and NOD.DKO) remained diabetes free (Fig. 7*E*), pointing to the indispensable role of IFN-γ signaling in anti–PD-1 diabetogenicity.

To exclude the role of IFN-γ signaling in lymphocytes (especially T cells), NOD. IFNγR1$^{-/-}$ Rag1$^{-/-}$ were generated by crossing NOD.IFNγR1$^{-/-}$ with NOD.Rag1$^{-/-}$ mice. Wild-type NOD splenocytes were transferred into NOD. IFNγR1$^{-/-}$ Rag1$^{-/-}$ and NOD.Rag1$^{-/-}$ recipients. After 4 wk of transfer, three doses of anti–PD-1 were given to the recipients and diabetes was followed for 4 wk. Upon PD-1 blockade, NOD splenocytes induced diabetes in NOD.Rag1$^{-/-}$ recipients rapidly but not in NOD. IFNγR1$^{-/-}$ Rag1$^{-/-}$ recipients (Fig. 7*F*), indicating that IFN-γ signaling in diabetogenesis was uncoupled from adaptive immunity and was dependent on innate immune system.

We examined whether increased NO resulting from iNOS activation would affect diabetogenesis mediated by anti–PD-1 treatment. Mice treated with anti–PD-1 antibody together with the iNOS inhibitor aminoguanidine (AG) were protected from acute diabetes induced by PD-1 blockade (Fig. 7*G*). Of note, the infiltration of MoMac was not affected by AG treatment, shown by the same ratio between MoMac and ReMac between anti–PD-1 alone treatment and combination of anti–PD-1 and AG treatment (Fig. 7 *H* and *I*), suggesting that the effect of NO in diabetes development was downstream of MoMac infiltration. Altogether, the findings indicated that the MoMac actively participate in the pathogenesis of autoimmune diabetes.

Activated Macrophages Are Cytotoxic to β-Cells. To test whether the activated macrophages can directly kill β-cells, we performed an ex vivo cytotoxicity assay consisting of coculturing a β-cell insulinoma line Min6 with activated macrophages obtained from the peritoneal cavity (*SI Appendix*, Fig. S7*A*). The macrophages were stimulated by culturing with LPS, IFN-γ, or a combination of LPS and IFN-γ. The expression of iNOS was induced by LPS and

increased by the combined treatment of LPS and IFN-γ (Fig. 8*A* and *SI Appendix*, Fig. S7*B*). Macrophages stimulated by both LPS and IFN-γ showed a dose-dependent cytocidal activity against β-cells, whereas macrophages activated by either LPS or IFN-γ alone did not (Fig. 8*B*). As a control, the viability of Min6 cells was not directly affected by culturing them with either of the treatments (*SI Appendix*, Fig. S7*C*). The cytocidal activity was contact-dependent as separation of macrophages from β-cells in a transwell failed to induce β-cell death (Fig. 8*C*). In contrast, macrophage stimulated with the combination of LPS and type I IFN IFN-β did not kill β-cells (Fig. 8*D*), suggesting the important role of IFN-γ. Indeed, macrophages deficient in *Ifngr1* in the presence of LPS and IFN-γ did not signal to induce iNOS (Fig. 8*E*) and failed to kill the β-cells (Fig. 8*F*). In agreement with the in vivo data, iNOS inhibition abolished the cytocidal activity of activated macrophages (Fig. 8*G*).

Discussion

Examining the acute diabetes that develops after checkpoint blockade of PD-1 allowed us to define critical cellular interactions taking place in islets. We confirm previous studies showing that PD-1 blockade but not CTLA-4 blockade induces acute diabetes development in adult mice (16). Loss or blockade of PD-1 signaling compressed diabetogenicity into a few days so cellular interactions were more clearly defined (14, 16). It led to the undisputed conclusion of the strong symbiosis between the intraislet T cells—both CD4 and CD8 were required—and the innate cellular system. We documented the presence of an exhausted subset of CD8 T cells that, remarkably, appeared very early in the development of this autoimmunity, was functionally reversed by the anti–PD-1 treatment and was a major participant in the ensuing inflammatory reaction. Still, a notable observation was the documentation that the final effector reaction leading to the demise of β-cells, derived from activated MoMac: Depleting them markedly reduced diabetogenesis.

Diabetes autoimmunity in both human and NOD mice is highly dependent for its initiation on recognition by CD4 T cells of β-cell–derived peptides presented on unique alleles of MHC-II proteins, I-A^{g7} in the case of NOD mice (43). CD4 T cells set

Fig. 7. Decreasing the infiltration of MoMac into islets prevents diabetes following PD-1 blockade. (*A*) Flow cytometry analysis showing the effects of clodronate liposome treatment on islet myeloid cells. Results are representative of two independent experiments each with $n \geq 6$ mice. (*B*) Ratio between MoMac and ReMac in islets from the data of *A*. Untreated age-matched NOD mice ($n = 5$) were examined as control. ***$P = 0.0007$, *$P = 0.011$, n.s. = 0.0874. (*C*) Percentage of infiltrating CD45 leukocytes from the data of *A* and *B*. ***$P = 0.001$, *$P = 0.0496$, n.s. = 0.0991. (*D*) Diabetes incidence of NOD mice treated with anti–PD-1 plus PBS liposomes ($n = 13$, red) or anti–PD-1 plus clodronate liposomes ($n = 12$, blue) at 6 to 8 wk of age. ****$P < 0.0001$. Results are pooled from three independent experiments. (*E*) Diabetes incidence of four strains of mice (NOD [$n = 35$, blue], NOD.IFNαR1$^{-/-}$ [$n = 10$, red], NOD.IFNγR1$^{-/-}$ [$n = 17$, green], and NOD.DKO [$n = 13$, purple]) treated with three injections of anti–PD-1. Ages of the mice ranged from 5-wk old to 16-wk old. Mice were followed for diabetes incidence for 4 wk. ****$P < 0.0001$, n.s. = 0.1363. Results are pooled from three independent experiments. (*F*) Diabetes incidence of NOD. Rag1$^{-/-}$ recipients ($n = 14$, red) or NOD. IFNγR1$^{-/-}$ Rag1$^{-/-}$ recipients ($n = 17$, blue) transferred with NOD splenocytes (10^7 per mouse). Four weeks later the mice were treated with three injections of anti–PD-1 antibodies and monitored diabetes for 4 wk. ***$P = 0.0003$. (*G*) Diabetes incidence of NOD mice treated with anti–PD-1 plus AG (6 mg per mouse, $n = 13$, blue) every 12 h for 20 d or anti–PD-1 alone ($n = 9$, red) starting at 5 to 7 wk of age and followed for 4 wk. **$P = 0.004$. Results are pooled from two independent experiments. (*H*) Flow cytometry analysis showing the effects of AG treatment: 5- to 7-wk-old NOD mice were treated as in *G*. Four weeks later, islets from the two groups of mice were isolated and examined by flow analysis. Data are representative from $n = 4$ mice from two independent experiments. Two mice from each group are combined for analysis in second experiment. (*I*) Ratio between MoMac and ReMac in islets from the data of *H*. (Ctrl vs. anti-PD-1) **$P = 0.0026$, (Ctrl vs. anti-PD-1+AG) **$P = 0.0016$, n.s. = 0.8421.
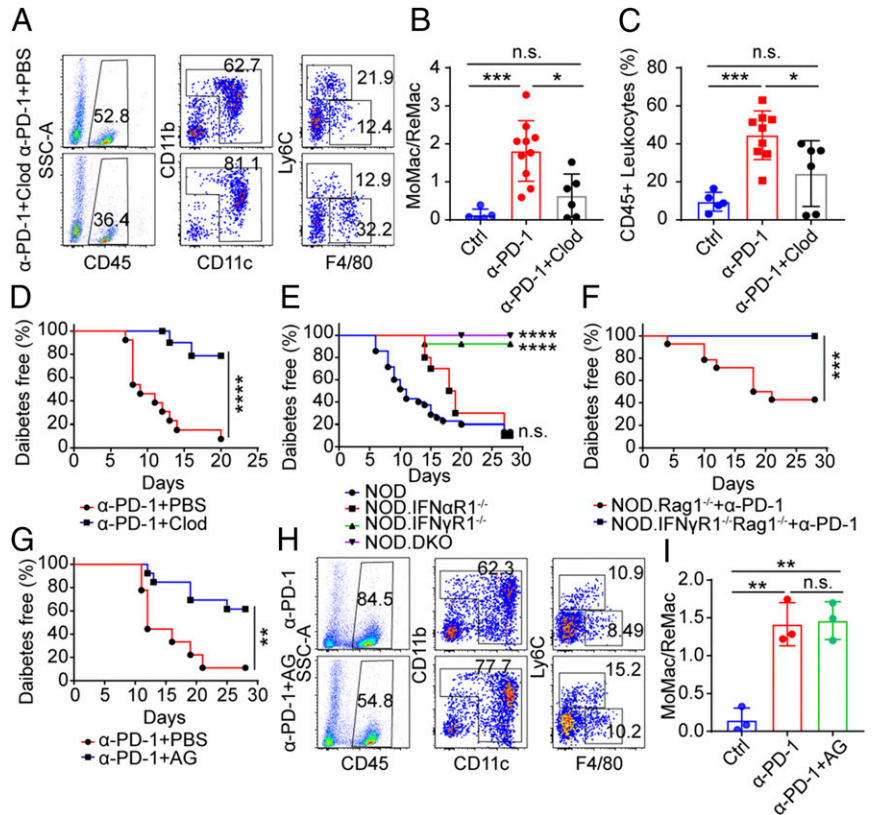
the autoimmune process in NOD by recognizing proinsulin derived peptides (44). Yet in NOD as in human T1D, CD8 T cells participate and play a significant role (19, 45, 46). We saw this symbiosis in the present experiments where depletion of either T cell affected anti–PD-1–mediated diabetes development. We envision a multistep reaction: An initial CD4 T cell in islets interacting with ReMac to be closely followed by entrance of DCs into islets, resulting in the recruitment and activation of CD8 T cells (47). Such interactions are subjected to ensuing with complex modulatory changes that determines the final outcome, the demise of β-cell mass.

We identified the heterogeneity of intraislet CD8 T cells that included the exhausted subset and documented their functional changes in response to PD-1 blockade. These findings in an autoimmune situation are consistent with those in chronic viral infection and cancer (29–31, 48). In our scRNA-seq data, a subset of CD8 T cells overexpressed *Tox*, an HMG-box transcription factor, the central regulator of the T "exhausted" cells. Another subset expressed additional high level of *Tcf-7*, identified as the precursor of the exhausted T cells. Those cells responded to anti–PD-1 treatment, leading to their high effector function, producing IFN-γ, and creating the proinflammatory milieu that resulted in a diabetic endpoint. An issue to note is the presence of these exhausted sets of T cells very early in the development of the autoimmune process, also indicated in our recent scRNA-seq analysis, as early as 8 wk of age (27). The obvious take-home message is that the islet microenvironment modulates the effector function of the initial autoreactive T cells. How this miniorgan, which consists of highly secretory β-cells, plus resident activated macrophages and activated endothelia regulate such T cell response, is a major issue to investigate.

A major effector cell leading to diabetes after PD-1 blockade was an activated MoMac, identified both by scRNA-seq analysis and flow cytometry. Their depletion reduced diabetes incidence. The MoMac in response to IFN-γ showed increased expression of MHC class II molecules and iNOS, that led to NO production and the killing of β-cells. These findings underscore two contrasting functions of the islet macrophages: Various subsets in an activated state having several functions, such as homeostatic, local defense, and antigen presentation; and the monocyte-derived, entering islets upon cues derived from an inflammatory state, and having a cytocidal role.

The findings on the cytocidal role of macrophages and their development requiring IFN-γ raise several important issues. First, what is their role and that of IFN-γ in regular diabetes? Early studies had pointed to the effector role of macrophages in NOD diabetes based on experiments depleting monocytes by clodronate liposomes administration or other treatments (49–52). (As shown here, clodronate liposome selectively depleted blood monocytes and did not affect the islets ReMac.) In the present analysis on islets from nonmanipulated NODs just before dysglycemia (*SI Appendix*, Fig. S4G), as well as in our recent scRNA-seq examination, the activated macrophages were strongly represented. Such subset was not found in the absence of IFN-γ receptor (27) but is highly represented in the present experiments with PD-1 blockade. This study shows that NOD.IFNγR1$^{-/-}$ and NOD.DKO female mice failed to respond to anti–PD-1 to induce acute diabetes; in striking contrast, spontaneous diabetes still developed in these mice, albeit with decreased incidence (53–55). This indicates alternative effector mechanisms during conventional diabetes, most likely pointing to CD8 cytolytic T cells.
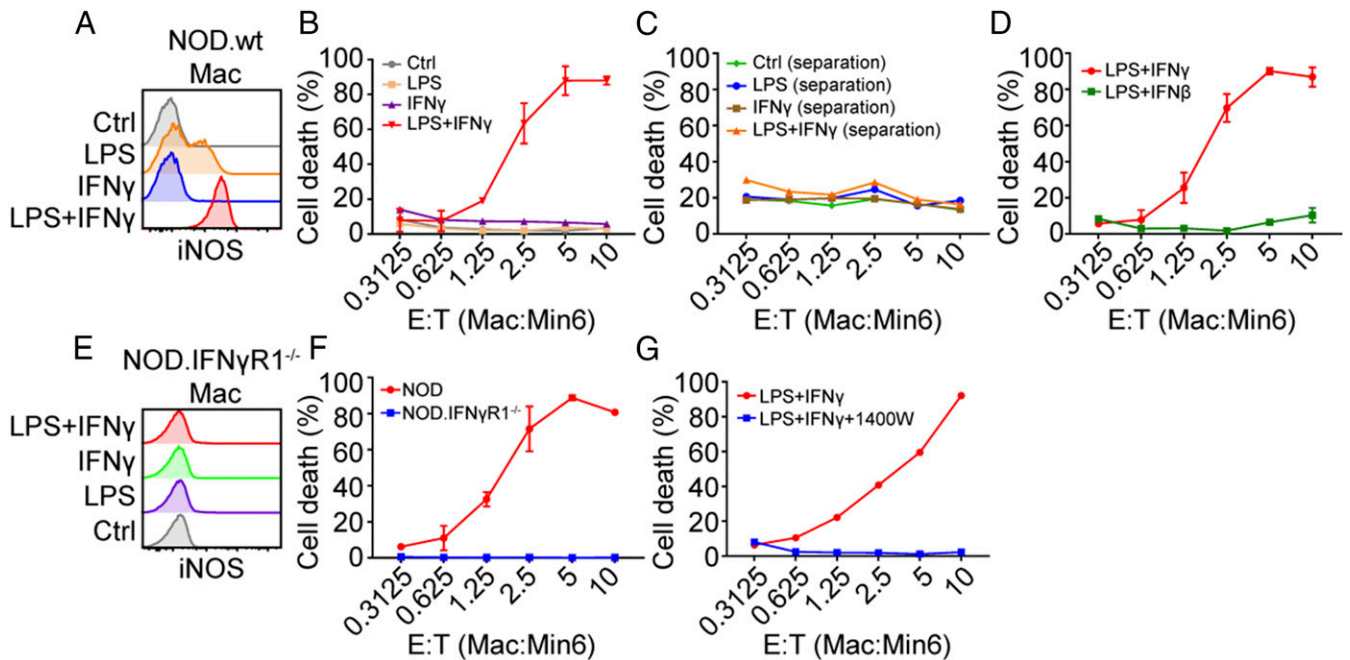
Fig. 8. Activated macrophages acquire cytocidal activity against β-cells. (*A*) Expression of iNOS in peritoneal macrophages treated with LPS (100 ng/mL) or IFN-γ (100 ng/mL) or a combination of both. Peritoneal macrophages were harvested from three 8- to 10-wk-old NOD mice and cultured with indicated reagents for 18 h after which the expression of iNOS was examined by flow cytometry. Data are representative from three independent experiments. (*B*) Cytotoxicity analysis of macrophages treated with different stimuli to β-cells (Min6) at various effector to target cell (E:T) ratios. Stimulated macrophages were washed and cultured with Min6 cells (50,000 cells per well) with different ratio as indicated and then cell death was examined by flow cytometry using fixable viability dye efluor 780. The same method to detect cytotoxicity of macrophages was used for *C, D, F,* and *G*. Results are pooled from two independent experiments. (*C*) Cytotoxicity analysis when separating macrophages from β-cells by a transwell. Results are pooled from two independent experiments. (*D*) Macrophages treated with LPS plus IFN-γ or LPS plus IFN-β (100 ng/mL) for 18 h for cytotoxicity assay. Results are pooled from two independent experiments. (*E*) Expression of iNOS in peritoneal macrophages from NOD.IFNγR1⁻/⁻ mice treated with various stimuli. Cells are harvested as in *A*. The experiment was performed one time. (*F*) Cytotoxicity analysis comparing NOD wild-type macrophages and IFNγR1⁻/⁻ macrophages. Results are pooled from two independent experiments. (*G*) Cytotoxicity analysis of NOD wild-type macrophages treated with NO inhibitor 1400W (100 μM). Results are pooled from two independent experiments.

Much discussion has taken place on the role of CD8 T cells and their association with β-cell killing. Diverse experimental manipulations have been tested, from gene knockouts of MHC-I on β-cells or APC, to gene knockouts of the cytolytic pathways in CD8 T cells, examining the roles of Fas-Fas-L and perforin-granzymes (56–59). While presentation by MHC-I peptide complex is absolutely required for diabetes progression, the association with direct cytolytic function may vary depending on the stage of the process. In our experiments we cannot exclude a role for CD8 T cells in direct killing of β-cells, a level of diabetes was still apparent after monocyte depletion. In such a complex and chronic autoimmune process, it is likely that several effector reactions may develop with time and contribute to the demise of β-cells.

Finally, our study opens the question of whether activated macrophages should be considered as the effector downstream of T cells in situations of checkpoint blockade in cancer and infectious diseases. Blockade of PD-1 signaling in the context of cancer and chronic infection has mostly focused on CD8 T cells. However, more recent studies are pointing to diverse roles of macrophages that supersedes their suppressive function. As for cancer, in a T3 MCA sarcoma mouse model, a subset of macrophages with both proinflammatory and monocyte signatures increased dramatically upon immune checkpoint blockade (60). Genetically, depletion of PD-1/PD-L1 signaling between T cells and macrophages favored a M1-associated macrophage signaling, including IL-6, TNFR, iNOS, and chemokine production (61). Blockade/deletion of PD-1 expression on tumor-associated macrophage restored phagocytosis, induced metabolic reprogramming of the macrophages, increased T cell effector function, promoted antigen presentation, and increased the survival of mice bearing

tumors (62, 63). Tumor-infiltrating macrophages expressed a high level of Trem2 that, when inhibited, modulated the tumor microenvironment, improved intratumoral T cell responses, and further augmented anti–PD-1 checkpoint immunotherapy (64, 65). To the extent that activated macrophages will be the final effector may much depend on the features of the particular cancer and its susceptibility to macrophage effector molecules.

In addition to cancer, PD-1 blockade had been largely studied in mouse models of LCMV infection where the role of cytolytic CD8 T cells is major component. Clinically, anti–PD-1 therapy has been tested to treat different chronic infectious diseases, resulting in enhanced immune responses against viruses and, in some cases, viral clearance (66–68). Thus, it will be an issue to consider whether besides T cells, activated macrophages also play a role in infectious diseases modulated by the PD-1 pathway. Paradoxically, PD-1 blockade induced macrophage activation leads to reactivation of *Mycobacterium tuberculosis* infection. The reactivation is dependent on augmented TNF-α secretion by macrophages (69). This would add another layer of complexity of targeting macrophages in the context of PD-1 blockade. Therefore, the biological effects of macrophage/monocyte activation downstream of PD-1 blockade are very much context-dependent. Hence, more efforts should be made to understand the biology of macrophages downstream of PD-1 blockade to uncouple their efficacy to complement therapeutics and toxicity to avoid adverse effects.

Materials and Methods

Mice. NOD/ShiLtJ (NOD), NOD.129S7(B6)-Rag1tm1Mom/J (NOD.*Rag1*⁻/⁻), and B6.NOD-(D17Mit21-D17Mit10)/LtJ (B6g7) were originally obtained from the

Jackson Laboratory; NOD.*Ifnar1*^−/−, NOD.*Ifngr1*^−/−, NOD.DKO (double knockout) (53), and NOD. *Ifngr1*^−/−. *Rag1*^−/− mice were generated in this study. All mice were bred and maintained and experimented in our pathogen-free animal facility in accordance with the Division of Comparative Medicine of Washington University School of Medicine (Association for Assessment and Accreditation of Laboratory Animal Care accreditation no. A3381-01).

Cell Line and Isolation of Peritoneal Macrophages. Insulinoma cell line, Min6, was obtained from ATCC and maintained in our laboratory in DMEM media supplemented with 15% FBS (vol/vol). Cell were propagated in vitro when the density of the cells reached 70% confluence. Peritoneal exudate cells were collected by flushing the peritoneum with 5 mL PBS with 2.5 mM EDTA and 0.2% BSA and cultured overnight, after which any lymphocytes were removed by extensive washing.

Treatment and Diabetes Monitoring. Mice were treated intraperitoneally with 250 μg anti–PD-1 (RMP1-14), anti–PD-L1 (10F.9G2), or anti–CTLA-4 (9D9) on days 0, 3, and 6. For controls, mice were injected with 200 μg of rat IgG2a isotype control antibody or PBS. Antibodies were diluted in PBS prior to injection for a total volume of 0.2 mL per mouse.

For CD4 T and CD8 T cell depletion, 250 μg of anti-CD4 (YTS177.1) and anti-CD8 (YTS169.4) were injected intraperitoneally 3 d before the first injection of anti–PD-1 and during the three doses of anti–PD-1 injection.

For NOD splenocyte transfer, splenocytes from NOD (10- to 12-wk old) were harvested and red blood cells were lysed with ACK (Ammonium-Chloride-Potassium) Lysing Buffer. Cells were washed with DMEM plus 10% FBS once and then with PBS for twice. Single-cell suspension was made in PBS buffer and 10×10^6 cells were transferred in 100 μL into 8- to 10-wk-old NOD.*Rag1*^−/− recipients or NOD. *Ifngr1*^−/−. *Rag1*^−/− recipients.

For monocyte depletion, 100 μL per mouse clodronate liposome or PBS liposome were injected on days −3, 0, 3, and 6 intravenously and anti–PD-1 were given on days 0, 3, and 6.

For iNOS inhibition, AG (6 mg per mouse) diluted in PBS were injected twice a day intraperitoneally (0800 hours in the morning and 2000 hours in the evening) intraperitoneally starting from day 0 to day 8, then once a day from day 9 to 20 (0800 hours in the morning). Anti–PD-1 were injected on days 0, 3, and 6.

Blood glucose was monitored every day after the third dose of anti–PD-1 until days 20 to 40 or weekly after splenocyte adoptive transfer. After two consecutive readings of >250 mg/dL (Chemstrip 2GP; Roche Diagnostics), mice were considered diabetic.

FACS and Conventional Flow Cytometry. Pancreatic islets were isolated as described previously (70) and dispersed into single-cell suspension using nonenzymatic Cell Dissociation Solution (Sigma-Aldrich) for 3 min at 37 °C. To block Fc-receptors engaging, the cell suspensions were incubated at 4 °C for 15 min in PBS (pH 7.4) supplemented with 2% FBS and 50% of FC-block (made in-house). For surface staining, cells were incubated with fluorescently labeled antibodies (1:200 [vol/vol]) at 4 °C for 20 min. Cells were then washed and analyzed by flow cytometry or subjected to FACS sorting.

For staining of intracellular transcription factors, islet cells were stained with surface antibodies for 20 min, fixed, and permeabilized using Foxp3/Transcription factor staining buffer set (Thermo Fisher Scientific) per the manufacturer's instructions. Cells were reacted with FOXP3, TCF1, and TOX antibodies at room temperature for 30 min.

For intracellular cytokine and protein staining, isolated islets (∼100 islets per well in 96-well plate) were placed at 37 °C in DMEM, 10% FBS (GE Healthcare), anti-CD3ε (10 μg/mL), anti-CD28 (5 μg/mL), and 10 μg/mL Brefeldin A for 4 h for IFN-γ detection. For iNOS staining, no stimulation was needed. Islets were then dispersed and washed with PBS, 1% BSA, and the cell surface stained with fluorescent antibodies for 30 min at 4 °C. Then the cells were fixed and permeabilized using BD Fixation/Permeabilization Solution Kit (Thermo Fisher Scientific) according to the instruction. The cells then were stained with fluorescent antibodies recognizing intracellular proteins IFN-γ and iNOS for 30 min at 4 °C.

For BrdU incorporation assay, mice were treated intraperitoneally with 1 mg per mouse BrdU in PBS starting from day 0 to day 6. The mice were separated into anti–PD-1–treated group (three injections of anti–PD-1 were given on days 0, 3, and 6) and untreated group. At day 7, islets were isolated from the two groups and BrdU incorporation were assessed according to the manufacturer's instruction (BD Pharmingen).

All conventional flow cytometry was done on BD FACSCanto II (BD Biosciences) and all of the FACS sorting was done on BD FACSAria II sorter (BD Biosciences) and analyzed using FlowJo 10.0 software (Tree Star).

Histology. Pancreata were isolated, fixed in 10% formalin, embedded in paraffin, sectioned, and stained with H&E. Microscopy was performed, and images were collected on the NanoZoomer (Hamamatsu Photonics K.K.).

scRNA-Seq, Library Preparation, Alignment, and Analysis. The scRNA-seq analysis was performed on live islet CD45^+ leukocytes from 8-wk-old NOD female mice either untreated or treated with anti–PD-1, four to eight mice per one sample. After sorting, cells were loaded onto the Chromium Controller (10X Genomics) (71). The resulting samples were processed using the Chromium Single Cell 3′ Library & Gel Bead Kit (10X Genomics, v2) following the manufacturer's protocol. The libraries were sequenced on Illumina NovaSeq6000. The 10X Genomics Cell Ranger (v2.1.1) was used for raw reads mapping (GRCm38) and counting unique molecular identifiers. The library preparation and sequencing were done at the Genome Technology Access Center core facility (GTAC, Washington University in St. Louis, https://gtac.wustl.edu/). The 8-wk-old control sample was the same used in the time course data (27). The Seurat package (v2.3.4) (72) was used for heterogeneity analysis and differential expression analysis. The Wilcoxon rank sum test was used to identify differentially expressed genes. A canonical correlation analysis was run to align datasets using the RunCCA function. For DC analysis, the inflammatory-driven signal affecting separation by cell types was reduced before the clustering.

Cytotoxicity Assay. Cytotoxicity killing assay was performed using Min6 β-cell line as target cells and peritoneal exudate macrophages cells. The day before coculture, peritoneal cells were plated and treated with different stimulations: untreated, 100 ng/mL LPS, 100 ng/mL IFN-γ, 100 ng/mL IFN-β, LPS^+IFN-γ, or LPS^+IFN-β. β-cell line Min6 were plated at 50,000 cells per well and rested overnight. The next day, peritoneal cells were washed, and macrophages were collected and added to β-cells at various ratios starting from 10:1 (macrophage to β-cells). Twenty-four hours later the cells were stained with indicated antibodies at 37 °C for 20 min. To detect cell death, cell viability dye 780 (ebioscience) was used along with other markers including CD45, CD11b, I-A^g7, and iNOS to identify macrophages. Then the cells were washed at least three times with PBS and trypsinized and collected for cell death detection by flow cytometry.

Statistical Analysis. Paired or unpaired two-tailed Student's *t* tests were performed when two groups of samples were compared. A Mantel–Cox log-rank test was performed to compare survival curves in mice from different treatment. All of the *P* values were calculated using GraphPad PRISM 7 with the following significance: n.s., $P > 0.05$; *$P < 0.05$; **$P < 0.01$; ***$P < 0.001$; ****$P < 0.0001$. Statistical details for each experiment can be found in the figures and legends.

1. M. Sznol *et al.*, Endocrine-related adverse events associated with immune checkpoint blockade and expert insights on their management. *Cancer Treat. Rev.* **58**, 70–76 (2017).
2. M. Mellati *et al.*, Anti-PD-1 and anti-PDL-1 monoclonal antibodies causing type 1 diabetes. *Diabetes Care* **38**, e137–e138 (2015).
3. J. Hughes *et al.*, Precipitation of autoimmune diabetes with anti-PD-1 immunotherapy. *Diabetes Care* **38**, e55–e57 (2015).
4. Z. Quandt, A. Young, M. Anderson, Immune checkpoint inhibitor diabetes mellitus: A novel form of autoimmune diabetes. *Clin. Exp. Immunol.* **200**, 131–140 (2020).

5. E. Ahn *et al.*, Role of PD-1 during effector CD8 T cell differentiation. *Proc. Natl. Acad. Sci. U.S.A.* **115**, 4749–4754 (2018).

6. K. J. Oestreich, H. Yoon, R. Ahmed, J. M. Boss, NFATc1 regulates PD-1 expression upon T cell activation. *J. Immunol.* **181**, 4832–4839 (2008).

7. Y. Agata *et al.*, Expression of the PD-1 antigen on the surface of stimulated mouse T and B lymphocytes. *Int. Immunol.* **8**, 765–772 (1996).

8. M. Hashimoto *et al.*, CD8 T cell exhaustion in chronic infection and cancer: Opportunities for interventions. *Annu. Rev. Med.* **69**, 301–318 (2018).

9. L. M. McLane, M. S. Abdel-Hakeem, E. J. Wherry, CD8 T cell exhaustion during chronic viral infection and cancer. *Annu. Rev. Immunol.* **37**, 457–495 (2019).

10. D. Moskophidis, F. Lechner, H. Pircher, R. M. Zinkernagel, Virus persistence in acutely infected immunocompetent mice by exhaustion of antiviral cytotoxic effector T cells. *Nature* **362**, 758–761 (1993).

11. A. J. Zajac *et al.*, Viral immune evasion due to persistence of activated T cells without effector function. *J. Exp. Med.* **188**, 2205–2213 (1998).

12. A. Schietinger *et al.*, Tumor-specific T cell dysfunction is a dynamic antigen-driven differentiation program initiated early during tumorigenesis. *Immunity* **45**, 389–401 (2016).

13. E. J. Wherry, J. N. Blattman, K. Murali-Krishna, R. van der Most, R. Ahmed, Viral persistence alters CD8 T-cell immunodominance and tissue distribution and results in distinct stages of functional impairment. *J. Virol.* **77**, 4911–4927 (2003).

14. J. Wang *et al.*, Establishment of NOD-Pdcd1–/– mice as an efficient animal model of type I diabetes. *Proc. Natl. Acad. Sci. U.S.A.* **102**, 11823–11828 (2005).

15. B. T. Fife *et al.*, Insulin-induced remission in new-onset NOD mice is maintained by the PD-1-PD-L1 pathway. *J. Exp. Med.* **203**, 2737–2747 (2006).

16. M. J. I. Ansari *et al.*, The programmed death-1 (PD-1) pathway regulates autoimmune diabetes in nonobese diabetic (NOD) mice. *J. Exp. Med.* **198**, 63–69 (2003).

17. K. E. Pauken, M. K. Jenkins, M. Azuma, B. T. Fife, PD-1, but not PD-L1, expressed by islet-reactive CD4+ T cells suppresses infiltration of the pancreas during type 1 diabetes. *Diabetes* **62**, 2859–2869 (2013).

18. K. E. Pauken *et al.*, Cutting edge: Identification of autoreactive CD4+ and CD8+ T cell subsets resistant to PD-1 pathway blockade. *J. Immunol.* **194**, 3551–3555 (2015).

19. H. Okamura *et al.*, PD-1 aborts the activation trajectory of autoreactive CD8+ T cells to prohibit their acquisition of effector functions. *J. Autoimmun.* **105**, 102296 (2019).

20. K. C. Osum *et al.*, Interferon-gamma drives programmed death-ligand 1 expression on islet β cells to limit T cell function during autoimmune diabetes. *Sci. Rep.* **8**, 8295 (2018).

21. M. E. Keir *et al.*, Tissue expression of PD-L1 mediates peripheral T cell tolerance. *J. Exp. Med.* **203**, 883–895 (2006).

22. J. A. Carrero *et al.*, Resident macrophages of pancreatic islets have a seminal role in the initiation of autoimmune diabetes of NOD mice. *Proc. Natl. Acad. Sci. U.S.A.* **114**, E10418–E10427 (2017).

23. J. F. Mohan *et al.*, Unique autoreactive T cells recognize insulin peptides generated within the islets of Langerhans in autoimmune diabetes. *Nat. Immunol.* **11**, 350–354 (2010).

24. M. Nakayama *et al.*, Prime role for an insulin epitope in the development of type 1 diabetes in NOD mice. *Nature* **435**, 220–223 (2005).

25. B. J. Miller, M. C. Appel, J. J. O'Neil, L. S. Wicker, Both the Lyt-2+ and L3T4+ T cell subsets are required for the transfer of diabetes in nonobese diabetic mice. *J. Immunol.* **140**, 52–58 (1988).

26. A. Bendelac, C. Carnaud, C. Boitard, J. F. Bach, Syngeneic transfer of autoimmune diabetes from diabetic NOD mice to healthy neonates. Requirement for both L3T4+ and Lyt-2+ T cells. *J. Exp. Med.* **166**, 823–832 (1987).

27. P. N. Zakharov, H. Hu, X. Wan, E. R. Unanue, Single-cell RNA sequencing of murine islets shows high cellular complexity at all stages of autoimmune diabetes. *J. Exp. Med.* **217**, e20192362 (2020).

28. D. L. Barber *et al.*, Restoring function in exhausted CD8 T cells during chronic viral infection. *Nature* **439**, 682–687 (2006).

29. F. Alfei *et al.*, TOX reinforces the phenotype and longevity of exhausted T cells in chronic viral infection. *Nature* **571**, 265–269 (2019).

30. O. Khan *et al.*, TOX transcriptionally and epigenetically programs CD8+ T cell exhaustion. *Nature* **571**, 211–218 (2019).

31. A. C. Scott *et al.*, TOX is a critical regulator of tumour-specific T cell differentiation. *Nature* **571**, 270–274 (2019).

32. S. J. Im, B. T. Konieczny, W. H. Hudson, D. Masopust, R. Ahmed, PD-1+ stemlike CD8 T cells are resident in lymphoid tissues during persistent LCMV infection. *Proc. Natl. Acad. Sci. U.S.A.* **117**, 4292–4299 (2020).

33. S. J. Im *et al.*, Defining CD8+ T cells that provide the proliferative burst after PD-1 therapy. *Nature* **537**, 417–421 (2016).

34. D. T. Utzschneider *et al.*, T cell factor 1-expressing memory-like CD8(+) T cells sustain the immune response to chronic viral infections. *Immunity* **45**, 415–427 (2016).

35. A. Subramanian *et al.*, Gene set enrichment analysis: A knowledge-based approach for interpreting genome-wide expression profiles. *Proc. Natl. Acad. Sci. U.S.A.* **102**, 15545–15550 (2005).

36. W. H. Hudson *et al.*, Proliferating transitory T cells with an effector-like transcriptional signature emerge from PD-1+ stem-like CD8+ T cells during chronic infection. *Immunity* **51**, 1043–1058.e4 (2019).

37. Z. Chen *et al.*, TCF-1-centered transcriptional network drives an effector versus exhausted CD8 T cell-fate decision. *Immunity* **51**, 840–855.e5 (2019).

38. P. K. Gupta *et al.*, CD39 expression identifies terminally exhausted CD8+ T cells. *PLoS Pathog.* **11**, e1005177 (2015).

39. I. Siddiqui *et al.*, Intratumoral Tcf1+PD-1+CD8+ T cells with stem-like properties promote tumor control in response to vaccination and checkpoint blockade immunotherapy. *Immunity* **50**, 195–211.e10 (2019).

40. B. C. Miller *et al.*, Subsets of exhausted CD8+ T cells differentially mediate tumor control and respond to checkpoint blockade. *Nat. Immunol.* **20**, 326–336 (2019).

41. P. M. Odorizzi, K. E. Pauken, M. A. Paley, A. Sharpe, E. J. Wherry, Genetic absence of PD-1 promotes accumulation of terminally differentiated exhausted CD8+ T cells. *J. Exp. Med.* **212**, 1125–1137 (2015).

42. J. Gao, D. C. Morrison, T. J. Parmely, S. W. Russell, W. J. Murphy, An interferon-γ-activated site (GAS) is necessary for full expression of the mouse iNOS gene in response to interferon-γ and lipopolysaccharide. *J. Biol. Chem.* **272**, 1226–1230 (1997).

43. X. Wan *et al.*, The MHC-II peptidome of pancreatic islets identifies key features of autoimmune peptides. *Nat. Immunol.* **21**, 455–463 (2020).

44. X. Wan *et al.*, Pancreatic islets communicate with lymphoid tissues via exocytosis of insulin peptides. *Nature* **560**, 107–111 (2018).

45. M. E. Keir, G. J. Freeman, A. H. Sharpe, PD-1 regulates self-reactive CD8+ T cell responses to antigen in lymph nodes and tissues. *J. Immunol.* **179**, 5064–5070 (2007).

46. H. A. Abdelsamed *et al.*, Beta cell-specific CD8+ T cells maintain stem cell memory-associated epigenetic programs during type 1 diabetes. *Nat. Immunol.* **21**, 578–587 (2020).

47. S. T. Ferris *et al.*, A minor subset of Batf3-dependent antigen-presenting cells in islets of Langerhans is essential for the development of autoimmune diabetes. *Immunity* **41**, 657–669 (2014).

48. C. Yao *et al.*, Single-cell RNA-seq reveals TOX as a key regulator of CD8+ T cell persistence in chronic infection. *Nat. Immunol.* **20**, 890–901 (2019).

49. H.-S. Jun, C.-S. Yoon, L. Zbytnuik, N. van Rooijen, J.-W. Yoon, The role of macrophages in T cell-mediated autoimmune diabetes in nonobese diabetic mice. *J. Exp. Med.* **189**, 347–358 (1999).

50. H. S. Jun, P. Santamaria, H. W. Lim, M. L. Zhang, J. W. Yoon, Absolute requirement of macrophages for the development and activation of beta-cell cytotoxic CD8+ T-cells in T-cell receptor transgenic NOD mice. *Diabetes* **48**, 34–42 (1999).

51. K.-U. Lee, K. Amano, J.-W. Yoon, Evidence for initial involvement of macrophage in development of insulitis in NOD mice. *Diabetes* **37**, 989–991 (1988).

52. B. Calderon, A. Suri, E. R. Unanue, In CD4+ T-cell-induced diabetes, macrophages are the final effector cells that mediate islet β-cell killing: Studies from an acute model. *Am. J. Pathol.* **169**, 2137–2147 (2006).

53. J. A. Carrero, N. D. Benshoff, K. Nalley, E. R. Unanue, I. Type, Type I and II interferon receptors differentially regulate type 1 diabetes susceptibility in male versus female NOD mice. *Diabetes* **67**, 1830–1835 (2018).

54. D. V. Serreze *et al.*, Interferon-gamma receptor signaling is dispensable in the development of autoimmune type 1 diabetes in NOD mice. *Diabetes* **49**, 2007–2011 (2000).

55. B. Hultgren, X. Huang, N. Dybdal, T. A. Stewart, Genetic absence of gamma-interferon delays but does not prevent diabetes in NOD mice. *Diabetes* **45**, 812–817 (1996).

56. E. E. Hamilton-Williams, S. E. Palmer, B. Charlton, R. M. Slattery, Beta cell MHC class I is a late requirement for diabetes. *Proc. Natl. Acad. Sci. U.S.A.* **100**, 6688–6693 (2003).

57. N. L. Dudek *et al.*, Cytotoxic T-cells from T-cell receptor transgenic NOD8.3 mice destroy β-cells via the perforin and Fas pathways. *Diabetes* **55**, 2412–2418 (2006).

58. V. Varanasi, L. Avanesyan, D. M. Schumann, A. V. Chervonsky, Cytotoxic mechanisms employed by mouse T cells to destroy pancreatic β-cells. *Diabetes* **61**, 2862–2870 (2012).

59. Z. U. Mollah *et al.*, Granzyme B is dispensable in the development of diabetes in nonobese diabetic mice. *PLoS One* **7**, e40357 (2012).

60. M. M. Gubin *et al.*, High-dimensional analysis delineates myeloid and lymphoid compartment remodeling during successful immune-checkpoint cancer therapy. *Cell* **175**, 1014–1030.e19 (2018).

61. B. Diskin *et al.*, PD-L1 engagement on T cells promotes self-tolerance and suppression of neighboring macrophages and effector T cells in cancer. *Nat. Immunol.* **21**, 442–454 (2020).

62. S. R. Gordon *et al.*, PD-1 expression by tumour-associated macrophages inhibits phagocytosis and tumour immunity. *Nature* **545**, 495–499 (2017).

63. L. Strauss *et al.*, Targeted deletion of PD-1 in myeloid cells induces antitumor immunity. *Sci. Immunol.* **5**, eaay1863 (2020).

64. M. Molgora *et al.*, TREM2 modulation remodels the tumor myeloid landscape enhancing anti-PD-1 immunotherapy. *Cell* **182**, 886–900.e17 (2020).

65. Y. Katzenelenbogen *et al.*, Coupled scRNA-seq and intracellular protein activity reveal an immunosuppressive role of TREM2 in cancer. *Cell* **182**, 872–885.e19 (2020).

66. C. L. Day *et al.*, PD-1 expression on HIV-specific T cells is associated with T-cell exhaustion and disease progression. *Nature* **443**, 350–354 (2006).

67. E. E. West *et al.*, PD-L1 blockade synergizes with IL-2 therapy in reinvigorating exhausted T cells. *J. Clin. Invest.* **123**, 2604–2615 (2013).

68. D. Gardiner *et al.*, A randomized, double-blind, placebo-controlled assessment of BMS-936558, a fully human monoclonal antibody to programmed death-1 (PD-1), in patients with chronic hepatitis C virus infection. *PLoS One* **8**, e63818 (2013).

69. L. B. Tezera *et al.*, Anti-PD-1 immunotherapy leads to tuberculosis reactivation via dysregulation of TNF-α. *eLife* **9**, e52668 (2020).

70. B. Calderon *et al.*, The pancreas anatomy conditions the origin and properties of resident macrophages. *J. Exp. Med.* **212**, 1497–1512 (2015).

71. G. X. Y. Zheng *et al.*, Massively parallel digital transcriptional profiling of single cells. *Nat. Commun.* **8**, 14049 (2017).

72. R. Satija, J. A. Farrell, D. Gennert, A. F. Schier, A. Regev, Spatial reconstruction of single-cell gene expression data. *Nat. Biotechnol.* **33**, 495–502 (2015).